Structures of Purine Nucleoside Phosphorylase from *Mycobacterium tuberculosis* in Complexes with Immucillin-H and Its Pieces†

Wuxian Shi,‡ Luiz A. Basso,§ Diogenes S. Santos,§ Peter C. Tyler,|| Richard H. Furneaux,|| John S. Blanchard,‡ Steven C. Almo,*,‡ and Vern L. Schramm*,‡

Department of Biochemistry, Albert Einstein College of Medicine, 1300 Morris Park Avenue, Bronx, New York 10461, Carbohydrate Chemistry Team, Industrial Research, Ltd., Lower Hutt, New Zealand, and Departamento de Biologia Molecular e Biotecnologia, Universidade Federal do Rio Grande do Sul, Avenida Bento Goncalves 9500, Porto Alegre-RS 91501-970, Brazil

Received March 23, 2001

ABSTRACT: A structural genomics comparison of purine nucleoside phosphorylases (PNPs) indicated that the enzyme encoded by *Mycobacterium tuberculosis* (TB-PNP) resembles the mammalian trimeric structure rather than the bacterial hexameric PNPs. The crystal structure of *M. tuberculosis* PNP in complex with the transition-state analogue immucillin-H (ImmH) and inorganic phosphate was solved at 1.75 Å resolution and confirms the trimeric structure. Binding of the inhibitor occurs independently at the three catalytic sites, unlike mammalian PNPs which demonstrate negative cooperativity in ImmH binding. Reduced subunit interface contacts for TB-PNP, compared to the mammalian enzymes, correlate with the loss of the cooperative inhibitor binding. Mammalian and TB-PNPs both exhibit slow-onset inhibition and picomolar dissociation constants for ImmH. The structure supports a catalytic mechanism of reactant destabilization by neighboring group electrostatic interactions, transition-state stabilization, and leaving group activation. Despite an overall amino acid sequence identity of 33% between bovine and TB-PNPs and almost complete conservation in active site residues, one catalytic site difference suggests a strategy for the design of transition-state analogues with specificity for TB-PNP. The structure of TB-PNP was also solved to 2.0 Å with 9-deazahypoxanthine (9dHX), iminoribitol (IR), and PO_4 to reconstruct the ImmH complex with its separate components. One subunit of the trimer has 9dHX, IR, and PO_4 bound, while the remaining two subunits contain only 9dHX. In the filled subunit, 9dHX retains the contacts found in the ImmH complex. However, the region of IR that corresponds to the oxocarbenium ion is translocated in the direction of the reaction coordinate, and the nucleophilic phosphate rotates away from the IR group. Loose packing of the pieces of ImmH in the catalytic site establishes that covalent connectivity in ImmH is required to achieve the tightly bound complex.

Tuberculosis causes 8 million new infections and kills 2 million people each year worldwide according to the World Health Organization (*1*). It is estimated that approximately 1 billion individuals, one-third of the world population, is infected with latent TB. The *Mycobacterium tuberculosis* genome project has completed the entire sequences for H37Rv, a laboratory strain, and for CDC1551, a strain isolated from a patient with tuberculosis (*2*, *3*). Analysis of the open reading frames predicted that these organisms express purine nucleoside phosphorylase (PNP). The enzyme catalyzes the phosphorolysis of purine nucleosides and deoxynucleosides to the corresponding purine bases and (deoxy)ribosyl 1-phosphate and plays a central role in purine recycling and salvage. PNP deficiency in humans causes T-cell immune deficiency, but the role of PNP in the pathogenesis of tuberculosis is unknown (*4*). Inhibitors of human PNP are potential drugs for immune suppression in organ transplantation as well as for treating T-cell leukemias and type IV autoimmune diseases such as lupus, rheumatoid arthritis, and psoriasis (*5*, *6*).

Crystal structures of PNPs from several organisms can be categorized into trimeric and hexameric classes (*7*−*12*). The trimeric PNPs include all mammalian enzymes and some of the bacterial enzymes, and these exhibit greater than 30% sequence identity. *M. tuberculosis* PNP was proposed to belong to the trimeric class on the basis of 33% and 55% sequence identities to the trimeric enzymes from bovine spleen and *Cellullomonas* sp., respectively. It shows no apparent sequence homology to the *Escherichia coli* enzyme, a member of the hexameric class. Comparison of the structures from the two classes revealed that they share a common fold; however, the residues composing the catalytic site differ substantially (*11*).

The transition-state structure for the arsenolysis of inosine by bovine PNP has been solved by kinetic isotope effect experiments (*13*, *14*). The dissociative transition state exhibits

† This work was supported by research grants from the NIH (J.S.B., S.C.A. and V.L.S.), the New Zealand Foundation for Research, Science and Technology (P.C.T. and R.H.F.), and the CNPq and FAPERGS of Brazil (L.A.B. and D.S.S.).

* Corresponding authors: telephone, (718) 430-2746; fax, (718) 430-8565; e-mail, almo@aecom.yu.edu or vern@aecom.yu.edu.

‡ Albert Einstein College of Medicine.

§ Universidade Federal do Rio Grande do Sul.

|| Industrial Research, Ltd.

10.1021/bi010585p CCC: $20.00
Published on Web 06/19/2001

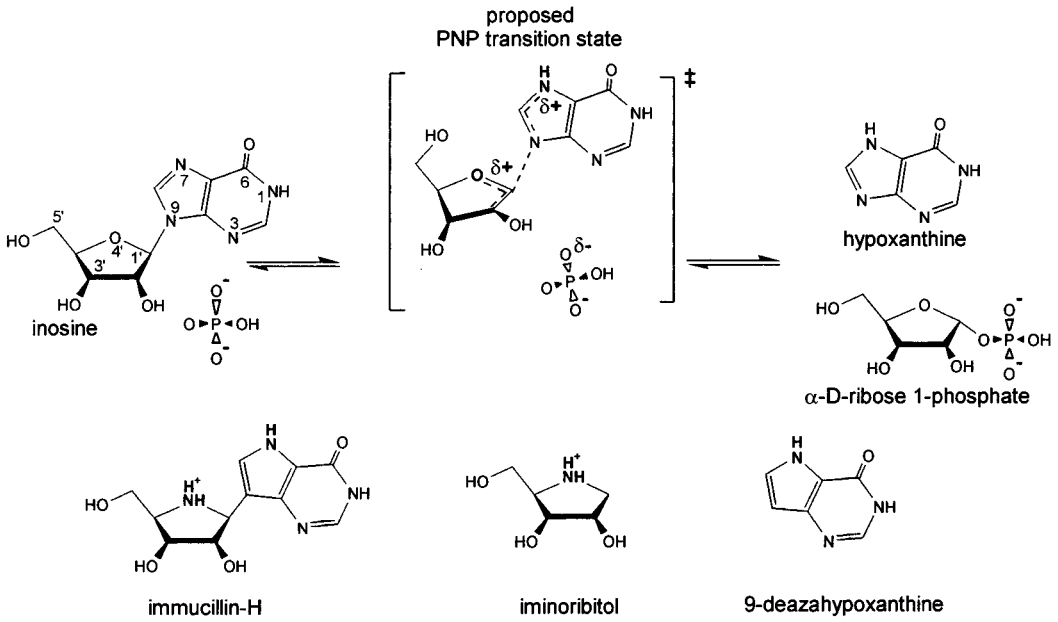

FIGURE 1: Reaction catalyzed by PNP. The oxocarbenium transition state is based on analysis of kinetic isotope effects for bovine PNP (*13*, *14*). The transition-state inhibitor ImmH is compared to the proposed transition-state complex. The iminoribitol ring of ImmH mimics the positive charge in the oxocarbenium-like transition state when protonated. The equilibrium binding constant for the inhibitor is 28 pM (*16*). Atomic numbering is indicated for inosine. The same numbering is used for ImmH in the text. The two pieces of ImmH, iminoribitol and 9-deazahypoxanthine, are shown in their protonated states. The neutral form of ImmH binds to the catalytic site of PNP and is proposed to be protonated during slow-onset binding (*16*).

oxocarbenium character with significant positive charge at the O4′−C1′ atoms of the ribose ring. Loss of the bonding electrons from C1′−N9 to the purine ring increases the pK_a of N7 and O6 of the purine. Immucillin-H (ImmH)[1] is a logically designed transition-state analogue that incorporates both of these stereoelectronic properties present in the transition state (*15*). The ribosyl O4′ oxygen is replaced with an imino group,[2] which can be protonated (pK_a ∼ 6.5) to form an imino cation to mimic the positive charge of the oxocarbenium transition state (Figure 1). Replacing N9 of the purine with carbon provides the chemically stable C−C ribosidic bond and increases the pK_a of N7 to 9.5.[3] Protonation of N7 and/or O6 is proposed to occur at the transition state. The equilibrium dissociation constants (K_i*) for ImmH with bovine spleen PNP and *M. tuberculosis* (TB) PNP are 23 and 28 pM, respectively, in the presence of phosphate. Thus, the binding is approximately 10^6 times tighter than substrate nucleosides (*15*, *16*). However, when the covalent C−C ribosidic bond of ImmH is removed, the component parts of 9dHX and IR bind with affinity similar to or weaker than the substrates (*16*). Here we characterize the basis for this difference by comparing the structure of TB-PNP in complex with ImmH and PO_4 to a structure with only 9dHX bound and to one with the component parts of ImmH bound separately in the complex of TB-PNP·9dHX·IR·PO_4.

The structures of TB-PNP in complex with the transition-state analogue ImmH and phosphate and with the individual components of ImmH permit dissection of the interaction between the PNP active site and this tight-binding transition-state analogue of the *M. tuberculosis* enzyme (*16*). The structure indicates that the oxocarbenium transition state for phosphorolysis of nucleosides is stabilized by an interaction with the 5′-hydroxyl neighboring group, demonstrating a substrate-assisted catalytic mechanism. Fifteen hydrogen bonds of 2.9 Å or less hold ImmH in a conformation favorable for oxocarbenium ion formation and hold phosphate in a position to react after transition-state formation. An enzymatically immobilized water molecule is proposed to act as a catalytic site acid to protonate the purine carbonyl O6 at the transition state. Weaker binding in the complex of TB-PNP·9dHx·IR·PO_4 reflects the loss of several H-bonds, increased separation between the active site participants, and increased mobility of catalytic site occupants. Despite a 33% amino acid identity between mammalian and TB-PNPs and the common trimeric structure, several differences in the binding of ImmH suggest that it may be possible to produce powerful transition-state analogues specific for TB-PNP.

METHODS

Crystallization of TB-PNP·ImmH·PO_4. Recombinant *M. tuberculosis* PNP was expressed and purified as described (*16*). The protein was cocrystallized with a 1:1.1 stoichiometry of ImmH and 5 mM inorganic phosphate by hanging-drop vapor diffusion at 18 °C. PNP protein (2 μL of 25 mg/mL) containing ImmH and 5 mM NaH_2PO_4 was mixed with an equal volume of the reservoir solution containing 100 mM Tris, pH 8.0, and 25% poly(ethylene glycol) 4000 and 25 mM $MgCl_2$ (Hampton) and equilibrated against 1.0 mL of the reservoir solution. Diffraction from the crystals was consistent with the space group $P3_221$ ($a = b = 102.625$ Å,

[1] Abbreviations: TB-PNP, purine nucleoside phosphorylase from *Mycobacterium tuberculosis*; ImmH, immucillin-H [(1*S*)-1-(9-deazahypoxanthin-9-yl)-1,4-dideoxy-1,4-imino-D-ribitol]; 9dHX, 9-deazahypoxanthine; IR, iminoribitol (1,4-dideoxy-1,4-iminoribitol); PEG, poly(ethylene glycol); TB-PNP·ImmH·PO_4, TB-PNP·9dHX·IR·PO_4, and TB-PNP·9dHX, complexes with the indicated components bound at the catalytic site(s).

[2] The original description of the synthesis and characterization of 1,4-dideoxy-1,4-iminoribitol used the imino nomenclature (*30*). The IUPAC recommendations permit both imino and amino designations for these molecules. Here we retain the original imino nomenclature.

[3] A. A. Sauve and V. L. Schramm, unpublished results.

$c = 128.478$ Å), with a trimer in the asymmetric unit ($V_m = 2.37$ Å^3/Da; 48% solvent content).

Crystallization of TB-PNP·9dHX·IR·PO$_4$. The enzyme was cocrystallized at 18 °C by hanging-drop vapor diffusion in the presence of a 1:1.5 stoichiometry of IR and 9dHX in 5 mM inorganic phosphate. The protein (2 μL of 25 mg/mL) containing IR, 9dHX, and 5 mM NaH_2PO_4 was placed onto a glass cover slip and mixed with an equal volume of the reservoir solution containing 100 mM Tris, pH 8.0, and 24% PEG 4000 and 25 mM $MgCl_2$ (Hampton) and was equilibrated against 1.0 mL of the reservoir solution. Diffraction was consistent with the orthorhombic $P2_12_12$ space group ($a = 119.984$ Å, $b = 135.773$ Å, $c = 45.012$ Å), with a trimer in the asymmetric unit ($V_m = 2.23$ Å^3/Da; 44% solvent content).

Data Collection, Processing, and Structure Determination. Crystals were cryoprotected by transfer to crystallization solution supplemented with 20% glycerol and flash cooled at −178 °C. X-ray diffraction data were collected at 0.98 Å wavelength on a 2 × 2 ADSC Quantum CCD detector using synchrotron radiation at beamline X9B at the National Synchrotron Light Source (Brookhaven National Laboratory). Data for TB-PNP·ImmH·PO$_4$ were reduced using the HKL package (*17*) and were 99.7% complete to 1.75 Å resolution with R_{sym} of 5.4%. In the last shell (1.81−1.75 Å), 84% of reflections had $I/\sigma(I) > 1.0$ with R_{sym} of 21.7%. The structure of *M. tuberculosis* PNP·ImmH·PO$_4$ was solved by molecular replacement with the AmoRe software package implemented in CCP4 (*18*) using the trimer of the *Cellulomonas* sp. PNP·iodoguanine complex as the search model (55% identity; *10*). The best solution after rigid-body refinement yielded an initial *R*-factor of 52.1% and a correlation coefficient of 45.3% using 8.0−4.0 Å data.

The data set for TB-PNP·9dHX·IR·PO$_4$ was 93.9% complete to 2.0 Å resolution with R_{sym} of 7.3%. In the last shell (2.07−2.00 Å), 68% of the reflections had $I/\sigma(I) > 1.0$. The structure of TB-PNP·9dHX·IR·PO$_4$ was solved by the molecular replacement method using the TB-PNP·ImmH·PO$_4$ complex as the search model. The best solution after rigid-body refinement yielded an initial *R*-factor of 39.4% using the 8.0−4.0 Å data.

Structure Refinement. The structures for both TB-PNP·ImmH·PO$_4$ and TB-PNP·9dHX·IR·PO$_4$ were refined using CNS (*19*). For TB-PNP·ImmH·PO$_4$, residues 233−255 were removed from the model in the early stage of refinement and built into unambiguous electron density in subsequent cycles using the program O (*20*). In addition, the loop segment (residues 62−66) not present in the starting model was also modeled into the electron density. The final model includes residues 7−268, ImmH, a phosphate ion for each monomer, and a total of 485 water molecules, with R_{cryst} and R_{free} of 18.9% and 21.2%, respectively. The model displays excellent stereochemistry as determined by PROCHECK (*21*), with 91.6% of the residues in the most favored region, 7.9% in additionally allowed region, and 0.5% in the disallowed region of the Ramachandran plot. Only Thr209 is in the disallowed region in all three monomers but demonstrates good density in the $F_o - F_c$ omit map. van der Waals contacts at subunit interfaces were identified by Contactsym (*22*). The structure has been deposited in the Protein Data Bank, PDB ID code 1G2O.

For refinement of TB-PNP·9dHX·IR·PO$_4$, the loop segments containing residues 61−70, 148−155, and 235−249 were subjected to extensive rebuilding in all three subunits. The final model includes residues 3−268, one IR, one 9dHX, and one PO_4 ion in subunit A, residues 6−268 and a 9dHX for subunit B, residues 7−268 and one 9dHX for subunit C, and a total of 274 water molecules, with R_{cryst} and R_{free} of 20.6% and 23.5%, respectively. The model displays excellent stereochemistry, with 91.2% in the most favored region, 8.3% in additionally allowed regions, and 0.5% in the disallowed region of the Ramachandran plot. Only Thr209 is in the disallowed region in all three monomers. These Ramachandran parameters are similar to those observed in the TB-PNP·ImmH·PO$_4$ complex. The structure has been deposited in the Protein Data Bank, PDB ID code 1I80.

RESULTS AND DISCUSSION

Overall Structure of TB-PNP·ImmH·PO$_4$. The complex is a symmetrical homotrimer with a triangular arrangement of subunits similar to the mammalian trimeric PNPs (*6*−*10*; Figure 2 a,b). The monomer of the complex is folded into a single domain structure containing eleven β strands and eight α helices (Figure 2a). The core consists of a mixed eight-stranded β sheet (β2, 49−52; β3, 71−76; β4, 81−86; β1, 28−34; β5, 112−124; β11, 221−233; β6, 132−136; and β8, 176−179). β5 and β11 are extended and participate in a smaller five-stranded β sheet (β11; β5; β10, 203−206; β9, 180−183; and β7, 137−142). The β sheet core is flanked by several α helices on each side (α1, 9−23; α2, 42−46; α3, 91−110; α4, 161−171; α5, 190−200; α6, 210−219; α7, 242−252; and α8, 254−267). The segment connecting β2 and β3 (residues 61−71) was disordered in the *Cellulomonas* PNP structure and was built into clear density in the $F_o - F_c$ electron density map. Residues from this segment do not interact directly with bound inhibitor or phosphate but are involved in orienting side chains of residues in the catalytic sites. In addition, the loop/helical segment (residues 236−253) moved considerably closer toward the active site, with Asn231 interacting with the 9dHX portion of bound ImmH.

The three subunits of the *M. tuberculosis* PNP trimer are related by a noncrystallographic 3-fold symmetry and display an RMS deviation of less than 0.3 Å for all Cα atoms in pairwise comparisons (Figure 2b). The sum of the trimer interface is extensive and buries a total of 5402 Å^2 surface area. Contacts between each subunit involve residues from α3 (residues 91−95), α5 (residues 185−200), and the loop connecting β11 to α7 (residues 239−243) from one subunit and β7−α4 (residues 138−157) from the adjacent subunit. The interface is stabilized by seven neutral hydrogen bonds and ten pairwise van der Waals interactions. The seven hydrogen bond interactions at the subunit interfaces include Tyr92A O−N Gly150B, His187A ND1−OG Ser146B, Tyr188A N−O Val154B, Leu241A N−OD1 Asp155B, Ala192A N−OD2 Asp138B, Thr190A OG−O His139B, and Glu193A OE2−N Asn141B. The hydrophobic van der Waals interactions involve the pairs Tyr92A-Phe153B, Tyr188A-Phe153B, His243A-Phe153B, His187A-Ile214B, His187A-Leu156B, Thr190A-Asp138B, Thr190A-His139B, Ala192A-Asp138B, Glu193A-Leu140B, and Met196A-Leu142B (Figure 2c).

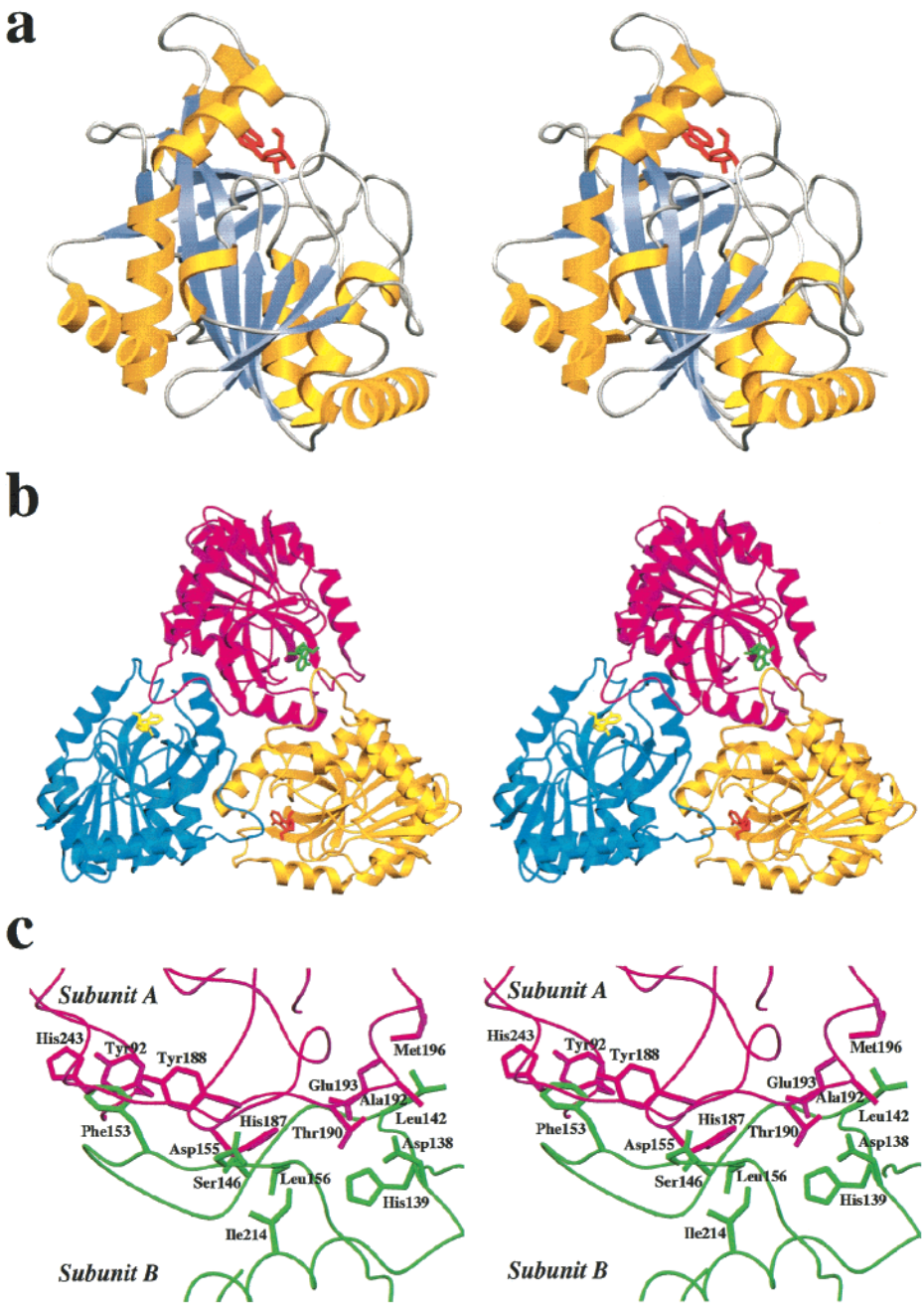

FIGURE 2: Stereo ribbon diagrams of *M. tuberculosis* PNP monomer with bound ImmH (a) and the trimer of the asymmetric unit (b). The active sites are located near the trimer interface. The catalytic site residues are amino acid contacts from a single subunit, except for Phe153 from a loop in the neighboring subunit. The subunit interface is shown with subunits A and B colored in magenta and green (c). Side chains displayed here are involved in hydrogen bond interactions and van der Waals contacts. This figure and Figures 3, 5, and 7 were generated using SETOR (*31*).

Interactions with the Transition-State Analogue ImmH. The three independent catalytic sites in the asymmetric unit are located near the subunit interfaces (Figure 2b). Each active site is composed of residues contributed almost entirely from a single subunit with the exception of Phe153, which is contributed from the adjacent subunit and participates in close hydrophobic interactions with C3′−C5′ of the iminoribitol group (Figure 3c). Phe153 stacks between Tyr92 and His243 in the active site. The structure shows that ImmH and phosphate fully occupy each monomer of the trimer with nearly identical geometries and contacts (Figure 3a). ImmH binds in the active site cleft between the small five-stranded β sheet (β11−β5−β10−β9−β7) and two helices (α5 and α7). Phosphate binds beneath the inhibitor close to the bottom of the active site and is a close neighbor to both C1′ and N4′ of the iminoribitol ring at 3.3 and 3.1 Å, respectively (Figure 4a). The 9dHX base of ImmH is wedged between the backbone of the small β sheet on one side and the side chain of Tyr188 from the other side (Figure 3c). The side chain of Asn231 forms hydrogen bonds with both the exocylic O6 and N7 of the 9dHX ring (2.8 and 3.0 Å, respectively). The same hydrogen bond pattern has also been observed in the complexes of bovine spleen PNP·ImmH·PO_4 (*9*) and PNP·hypoxanthine·ribose 1-phosphate (*8*). However, the hydrogen bond interactions are weaker in the Michaelis complex of the bovine spleen PNP·inosine·SO_4 structure, where these same distances increase to 3.3 and 3.4 Å, respectively. In the *Cellulomonas* PNP·5′-iodoguanine·

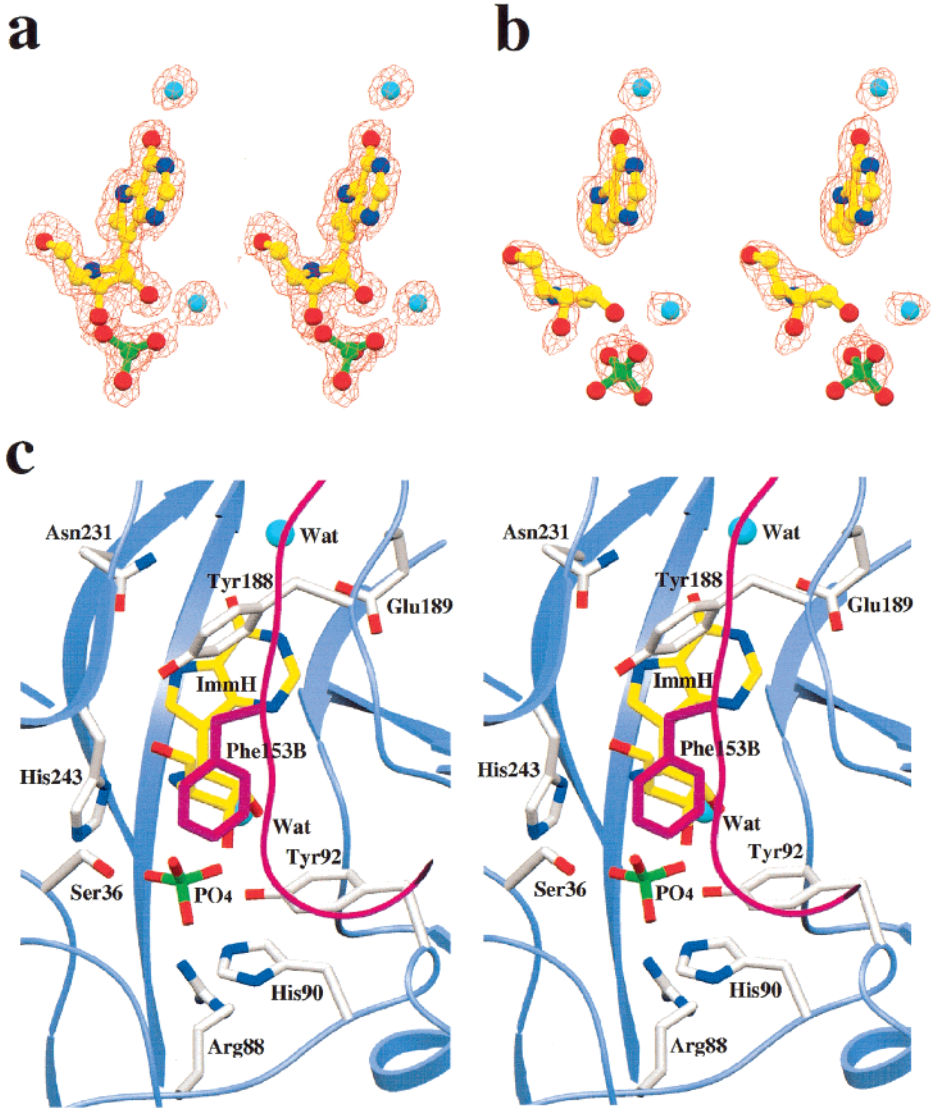

FIGURE 3: Stereoview of the $F_o - F_c$ electron density map contoured at 2σ for bound ImmH, phosphate, and two ordered water molecules (a). Stereoview of the $F_o - F_c$ electron density map contoured at 2σ for bound 9dHX, IR, and PO_4 (b). Stereoview of the active site of TB-PNP·ImmH·PO_4 (c). Asn231 hydrogen bonds with N7 and O6 of the 9-deazahypoxanthine ring of the inhibitor. Phe153B (shown in magenta) from the neighboring subunit interacts with C3′−C5′ of the bound inhibitor and stacks between Tyr92 and His243.

PO_4 structure, the equivalent of Asn231 is ~6 Å away from both O6 and N7 of the base analogue and participates in a water-mediated hydrogen bond with O6 (*10*).

Inosine at the transition state of the PNP reaction has significant oxocarbenium ion character with partial positive charge near O4′ on the ribose ring (*13*, *14*). The N4′ imino group of ImmH has a pK_a of 6.5 and can be protonated to mimic the localized positive charge of the transition state (*23*). Purine nucleosides and nucleotides prefer the C3′-*endo* conformation at the ground state (C3′ above the plane of the ribose ring). The transition state of bovine PNP has ribooxocarbenium ion properties and is characterized by a ribose ring with C1′ approaching sp^2 hybridization and a C3′-*exo* ribosyl ring pucker (C3′ below the plane; *23*−*25*). In the *M. tuberculosis* PNP complex, ImmH mimics this transition state characteristic with a C3′-*exo* pucker of the iminoribitol ring. A similar C3′-*exo* pucker has been observed in the complex of bovine PNP·ImmH·PO_4 and the human and *Plasmodium falciparum* hypoxanthine−guanine−xanthine phosphoribosyltransferase in complex with immucillin 5′-phosphates and Mg pyrophosphate (*26*, *27*).

The iminoribitol nitrogen of ImmH mimics the electronic charge feature of the oxocarbenium transition state in PNP but does not interact directly with any protein atoms (Figure 4a). Proposals for catalysis by transition-state stabilization anticipate enzymatic groups to interact with and to stabilize this transition-state feature. However, the nearest neighbors to the IR nitrogen include the O5′ from the inhibitor (2.7 Å) and O4 of the bound phosphate (3.1 Å) below the plane of the IR (Figure 4a). These interactions suggest electronic destabilization of the ground state by bringing three electron-rich oxygens into close proximity. Electrostatic stabilization of the O4′ oxocarbenium ion at the transition state would be favored by these same groups. The nearest oxygen of PO_4 is 3.3 Å from C1′, the site of nucleophilic displacement that occurs following transition-state formation (*13*, *14*). The purine base and phosphate are firmly anchored in the structure. Reaction coordinate motion for catalysis can be accommodated by translation of C1′ between N9 of the purine ring and O4 of the phosphate. Tyr92, together with the bound phosphate, orients the IR in the active site through interactions to the 2′- and 3′-hydroxyls.

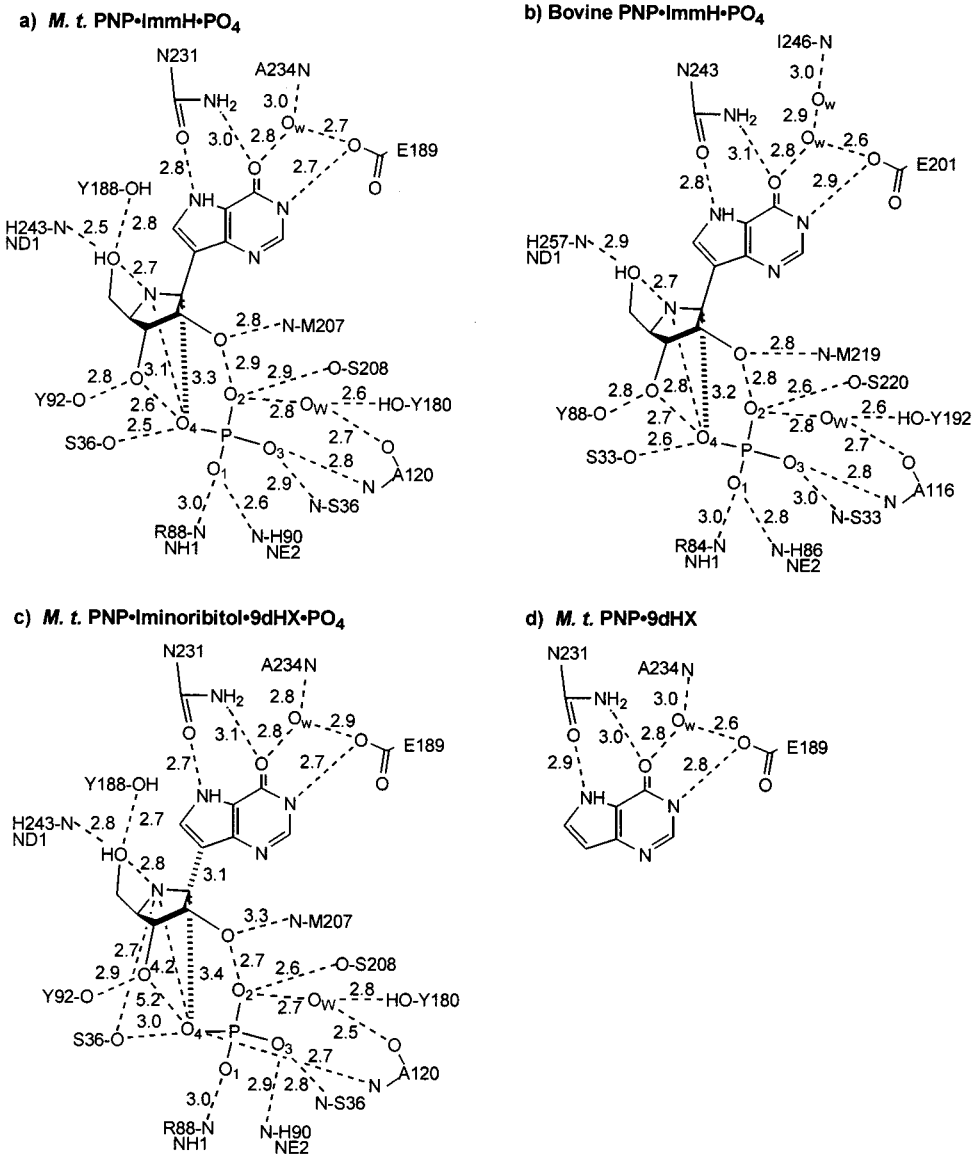

FIGURE 4: Distances (Å) for noncovalent interactions between the enzyme, phosphate, and ImmH in the complex with TB-PNP (a). Distances for the complex of bovine PNP•ImmH•PO_4 are shown in (b). Distances that define the interaction of TB-PNP•9dHX•IR•PO_4 are shown in (c). Two subunits of the TB-PNP complex crystallized in the presence of 9dHX, IR, and PO_4 contained only 9dHX. Its binding interactions with TB-PNP are shown in (d).

The 5′-hydroxyl group of ImmH is located close to α7 with His243 interacting through a 2.5 Å hydrogen bond. In addition, the edge of the phenolic ring in Tyr188 is oriented perpendicular to the plane of the ImmH base and also forms a 2.8 Å hydrogen bond with the 5′-hydroxyl (Figures 3c and 4a). Tyr188 is the only residue that interacts directly with bound inhibitor that is not conserved in the mammalian PNPs. This position is Phe in both human and bovine spleen PNPs and suggests that 5′ modifications of ImmH might be valuable in endowing specificity between mammalian and *M. tuberculosis* PNPs.

Phosphate Binding Site in TB-PNP•ImmH•PO_4. Phosphate binds beneath the inhibitor in the active site to stabilize the oxocarbenium transition state and orient the nucleoside substrate through interactions with the ribose moiety. All residues involved in phosphate binding are contributed from loops and provide a total of five direct hydrogen bonds and a sixth water-mediated hydrogen bond (Figure 4). Side chains of Arg88 and His90 hydrogen bond to O1 of the bound phosphate, while Ser36 interacts with both O4 and O3 through side chain and backbone atoms. The phosphate oxygen O2 is anchored by a direct hydrogen bond with the side chain of Ser208 and a water-mediated hydrogen bond with the backbone amide of Ala120 and the side chain hydoxyl of Tyr180. All residues participating in phosphate binding are conserved in the trimeric PNPs except Ala120, which provides a water-mediated hydrogen bond through a backbone amide group (Figure 4a,b).

Comparison of TB-PNP•ImmH•PO_4 with Other PNP Structures. The RMS deviation between Cα atoms of *M. tuberculosis* PNP and *Cellulomonas* PNP is 1.8 Å. However, the refined *M. tuberculosis* PNP structure is more similar to the bovine spleen PNP which has been crystallized with ImmH. The RMS deviation between Cα atoms is 1.4 Å for bovine and *M. tuberculosis* enzymes, even through the sequence homology between these two proteins is only 33% amino acid identity. The *M. tuberculosis* PNP shows substantial differences with the hexameric *E. coli* PNP

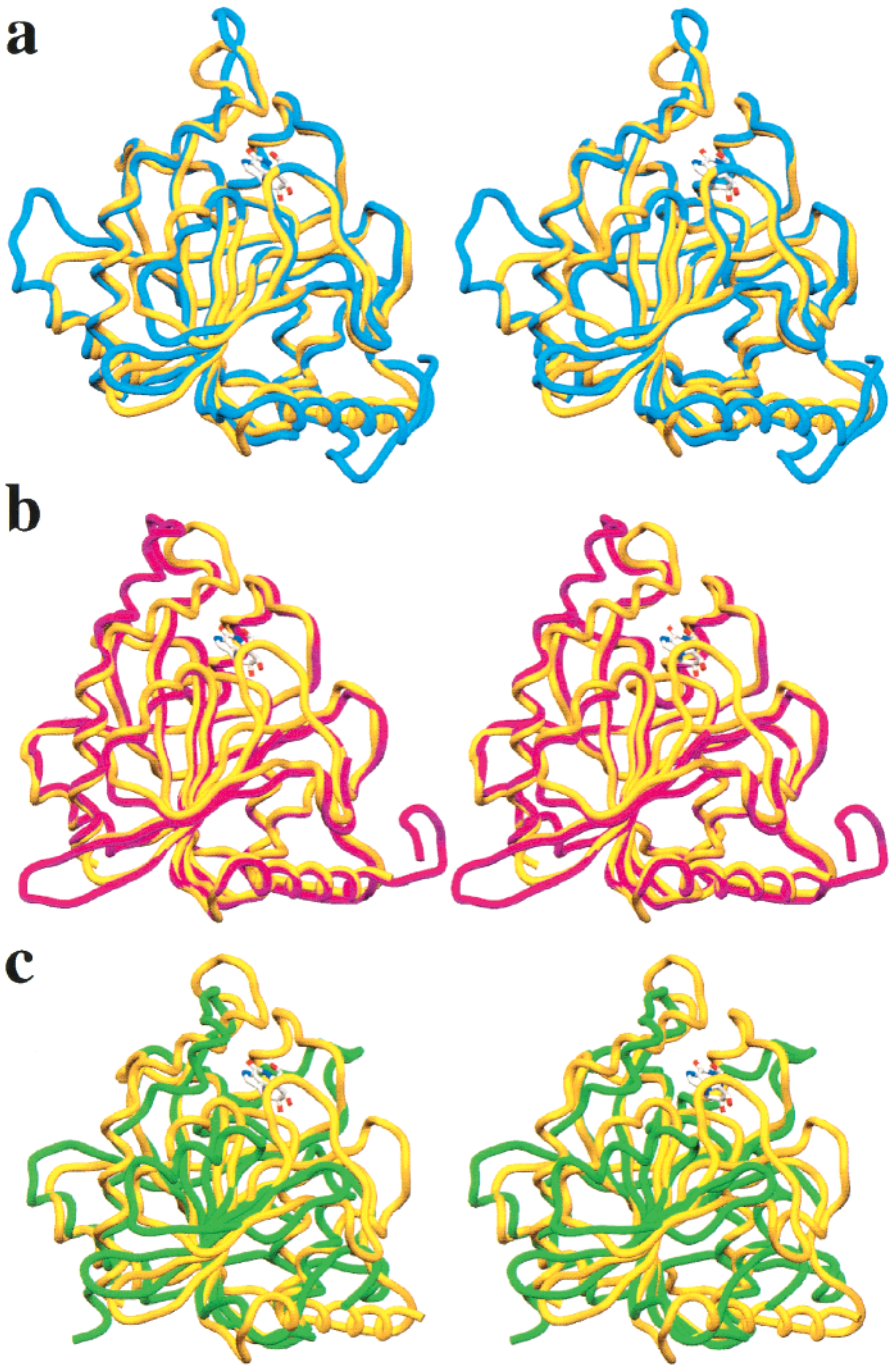

FIGURE 5: Superpositions of Cα atoms of the TB-PNP·ImmH·PO_4 complex (gold) with the bovine spleen PNP·ImmH·PO_4 complex (blue, PDB accession code 1B8O) in (a), with the *Cellulomonas* sp. PNP·iodoguanine·SO_4 complex (magenta, PDB accession code 1C3X) in (b), and with the *E. coli* PNP·formycin B·SO_4 complex (green, PDB accession code 1A69) in (c). *M. tuberculosis* PNP belongs to the trimeric class which includes mammalian PNP and *Cellulomonas* PNP.

enzyme, with a Cα RMS deviation of 3.2 Å (Figure 5c).

Bovine spleen PNP is known to use subunit-sequential catalysis, in which each catalytic site must react prior to its neighbor (*15*). Binding of ImmH at one of the three catalytic sites causes complete inhibition of catalysis. Strong negative cooperativity for inhibitor binding occurs to fill the remaining two sites of the trimer (*15*, *28*). *M. tuberculosis* PNP differs in having independent, identical binding of ImmH (*16*). The active sites of all known trimeric PNPs are located near the subunit interfaces. Catalytic site contacts in the *M. tuberculosis* enzyme come from a single subunit except for Phe153 (Phe159 in bovine PNP), contributed from the neighboring subunit to make van der Waals contacts with the hydrophobic face of the IR ring. In the complex of bovine PNP·ImmH·PO_4, additional hydrophobic contacts are observed between Phe159 with Val61 (Ala65 in *M. tuberculosis* PNP). The subunit interface contacts are more extensive in the bovine PNP complex, with 11 hydrogen bonds and 178 van der Waals interactions at each subunit interface, whereas only 7 direct hydrogen bonds and 140 van der Waals interactions are observed in the *M. tuberculosis* PNP complex. Only three of the hydrogen bonds involved in the trimer interface are conserved between bovine and *M. tuberculosis* PNPs. The residues involved in nonconserved hydrogen bonds at the

Table 1: Data Collection and Refinement Statistics

	PNP·ImmH·PO_4	PNP·9dHX·IR·PO_4
Data Collection		
resolution limits (Å)	20−1.75 (1.82−1.75)[a]	20−2.0 (2.07−2.00)
completeness (%)	99.7 (99.8)	93.9 (83.9)
R_{sym} (%)	5.4 (21.7)	7.3 (20.6)
no. of reflections		
unique	78938	48026
total	513786	176063
Structure Refinement		
R_{cryst} (%)	18.9	20.6
R_{free} (%)	21.2	23.5
no. of amino acids	783	788
no. of waters	485	274
no. of ligands	3 ImmH, 3 phosphate	3 9dHX, 1 iminoribitol, 1 phosphate
av protein *B*-factor (Å^2)	13.7	22.7
av ligand *B*-factor (Å^2)	8.6	23.2
av water *B*-factor (Å^2)	19.0	24.8
RMSD, bond (Å)	0.005	0.006
RMSD, angle (deg)	1.4	1.4

[a] Values in parentheses are for the highest resolution shell.

Table 2: Comparison of Hydrogen Bond Distances in Complexes of (**I**) TB-PNP·ImmH·PO_4, (**II**) TB-PNP·9dHX·IR·PO_4, and (**III**) Bovine PNP·ImmH·PO_4

atom 1	atom 2	residue	complex **I** (Å)	complex **II** (Å)	complex **III** (Å)
ImmH					
O5′	N4′	ImmH	2.7	2.8	2.7
	ND1	His243	2.5	2.8	2.9 (His257)
	OH	Tyr188	2.8	2.7	− (Phe200)
O3′	O4	PO_4	2.6		2.7
	OH	Tyr92	2.8	2.9	2.8 (Tyr88)
O2′	O2	PO_4	2.9	2.7	2.8
	N	Met207	2.8	3.3	2.8 (Met219)
N4′	O4	PO_4	3.1		2.8
	O5′	ImmH	2.7	2.8	2.7
	OG	Ser36		2.7	
N7	OD1	Asn231	2.8	2.7	2.8 (Asn243)
O6	ND2	Asn231	3.0	3.1	3.1 (Ans243)
N1	OH2	water	2.8	2.8	2.8
	OE2	Glu189	2.7	2.7	2.9 (Glu201)
PO_4					
O1	NE2	His90	2.6		2.8 (His86)
	NH1	Arg88	3.0	3.0	3.0 (Arg84)
O2	O2′	ImmH	2.8	2.7	2.8
	OG	Ser208	2.9	2.6	2.6 (Ser220)
	OH2	water	2.8	2.7	2.8
O3	N	Ala120	2.8		2.8 (Ala116)
	N	Ser36	2.9	2.8	3.0 (Ser33)
	NE2	His90		2.9	
O4	O3′	ImmH	2.6		2.7
	OG	Ser36	2.5	3.0	2.6 (Ser33)
	N4′	ImmH	3.1		2.8
	N	Ala120		2.7	

trimer interface in bovine PNP include Ser142, Asn145, Arg148, and Tyr249 (the equivalent of Thr143, Ser146, Val149, and Gly235 in *M. tuberculosis* PNP). These residues, in addition to Val61, are likely to play a role in the cooperative inhibitor binding and sequential catalytic action of bovine PNP.

Comparison of TB-PNP·ImmH·PO_4 and Bovine PNP·ImmH·PO_4. The catalytic sites of *M. tuberculosis* and bovine PNP complexes with ImmH and phosphate are similar but not identical (Table 2). A 2.8 Å hydrogen bond between Tyr188 and O5′ in *M. tuberculosis* PNP is prevented by a Phe in this position in the mammalian enzymes (Figure 4). Two water molecules are trapped in each active site of TB-PNP·ImmH·PO_4 and are located near phosphate O2 and O6 of the 9dHX. Three water molecules are located in each active site of the bovine PNP complex, with two water molecules equivalent to those described above but a third water molecule in the position occupied by the amide nitrogen of Ala234 in *M. tuberculosis* PNP. This water molecule in bovine PNP interacts with the amide nitrogen of Ile246 (Figure 4). The loop segment of residues 233−235 in the *M. tuberculosis* PNP complex is therefore closer to the bound inhibitor and creates a catalytic site that is more compact than that observed in the complex of bovine PNP·ImmH·PO_4.

The active sites of TB-PNP·ImmH·PO_4 and *Cellulomonas* PNP·5′-iodoguanine·SO_4 also show substantial differences. Most strikingly, several loops that are disordered or located distal from the active site in the *Cellulomonas* PNP structure move closer to the bound inhibitor and form an ordered and closed catalytic site in the TB-PNP complex. In TB-PNP, Asn231 forms direct hydrogen bonds with both O6 and N7 of 9dHX, whereas the equivalent residue Asn246 in *Cellulomonas* PNP interacts with O6 through a water-mediated hydrogen bond. These differences are presumably caused by the more favorable binding energy of the transition-state analogue inhibitor in TB-PNP. *Cellulomonas* PNP·5′-iodoguanine·SO_4 contains substrate analogues and is therefore more closely related to the Michaelis complex.

Structure of TB-PNP·9dHX·IR·PO_4. TB-PNP was also crystallized in the presence of the independent pieces of ImmH, namely, with 9dHX and IR in the presence of excess phosphate. The crystals diffracted well, and the structure was refined to 2.0 Å. One of the three active sites was filled with 9dHX, IR, and phosphate, while the remaining two sites were occupied only by 9dHX (Figures 4c and 6). Comparison of Cα atoms in the fully occupied subunit to those in the two partially filled subunits gave RMS deviations of 0.55 and 0.66 Å, respectively. The Cα atoms of the two subunits containing only 9dHX are somewhat more similar to each other, with an RMS deviation of 0.48 Å for all Cα atoms. Comparison of the subunit containing TB-PNP·9dHX·IR·PO_4 to the subunits of the TB-PNP·ImmH·PO_4 complex gives an RMS deviation of 0.58; thus the backbone and most side chains are similar. However, when the subunit of TB-PNP·9dHX·IR·PO_4 is compared to the two subunits containing only 9dHX, the RMS deviation increases to 0.78 and 0.92 Å, respectively, for all Cα atoms in the two subunits, even when excluding the phosphate binding loop composed of residues 61−70. This flexible loop contains three alanine and two glycine residues. In all three subunits of the TB-PNP·9dHX·IR·PO_4 complex, the loop is in an open conformation, showing relatively weak electron densities in the $2F_o - F_c$ map because it lacks stabilizing interactions with other parts of the structure. In the TB-PNP·ImmH·PO_4 complex, His68 from the loop shares hydrogen bonds with the side chain of Ser36 and the backbone atom of Arg88 (2.8 and 2.7 Å, respectively) and shares a stacking interaction with His90 (Figure 6b,c). Additional interactions from this loop include water-mediated hydrogen bonds between the amide nitrogen of Ala65 and the carbonyl oxygen of Arg88 and between the amide nitrogen of Thr64 and the carbonyl oxygen of Arg88.

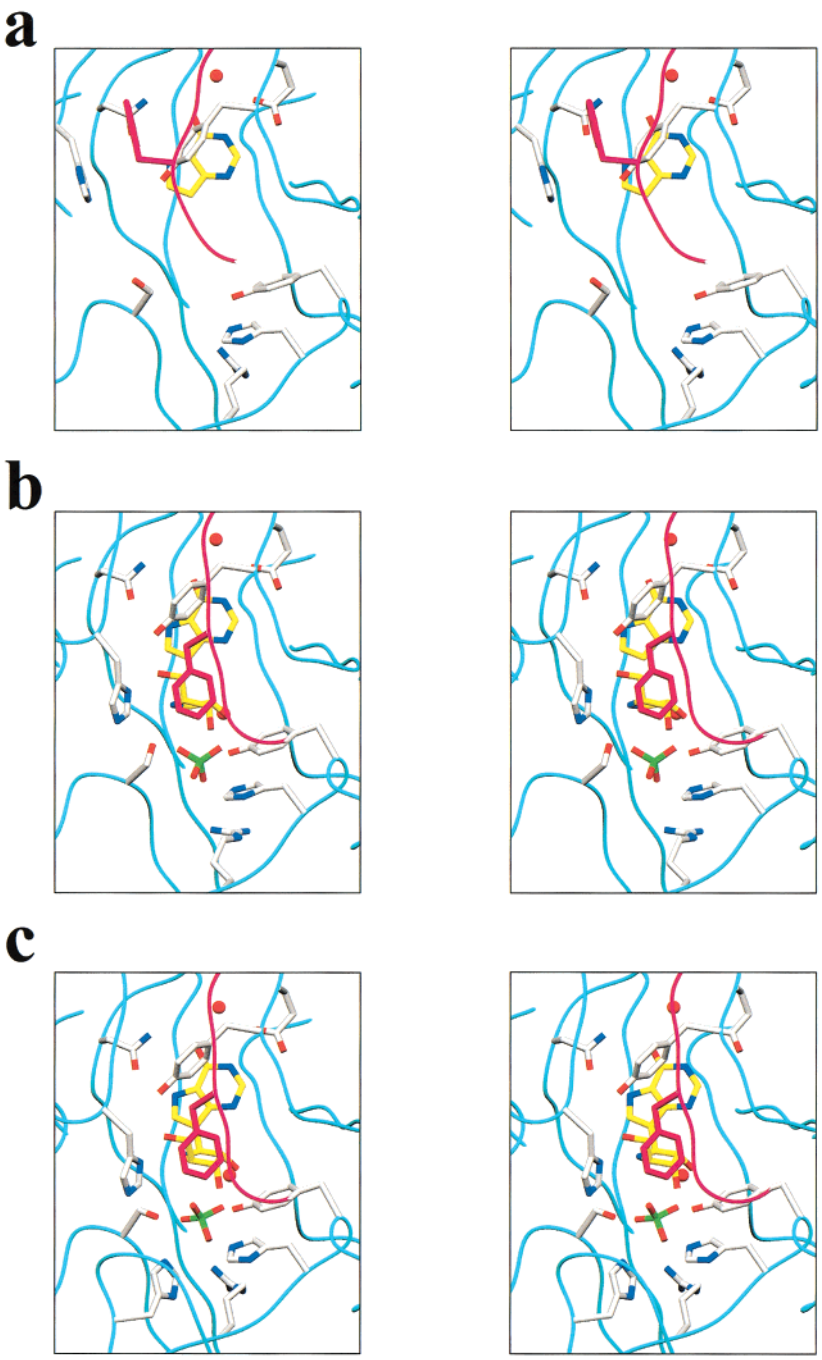

FIGURE 6: Stereoviews of the catalytic sites of TB-PNP with 9dHX alone (a), with the pieces of 9dHX, IR, and PO_4 (b), and with ImmH and PO_4 (c). Note the increased population of the site with polypeptide loops as the catalytic site is sequentially converted to the complex most closely related to the transition state (c). Water molecules are represented as red spheres. The five residues surrounding PO_4 in (c) are, from right to left, Tyr92, His90, Arg88, His68, and Ser36.

Binding of 9dHX. Two subunits in the TB-PNP·9dHX·IR·PO_4 complex contained only 9dHX (Figures 4a and 6d). Kinetic studies indicate a K_d of 0.39 μM for 9dHX, a 14 000-fold loss of binding affinity relative to the K_i* for ImmH (*16*). The 9dHX binds in the same position as in the complex of TB-PNP·9dHX·IR·PO_4, but the rest of the active site shows large differences in peptide geometry (Figure 6). The bidentate hydrogen bonds between Asn231 and N7 and O6 (2.9 and 3.0 Å) and between Glu189 (2.7 Å) and N1 of bound 9dHX are almost the same as in either complex of TB-PNP·9dHX·IR·PO_4 or TB-PNP·ImmH·PO_4 (Figure 4a,c). The water molecule that mediates contact between the O6 of 9dHX and the amide nitrogen of Ala234 is also conserved in all three complexes. This water molecule is proposed to act as a proton donor to activate the purine leaving group in bovine PNP (*9*).

Subunits filled with only 9dHX show changes in the active site loops that normally bind PO_4 and the ribosyl group. The 5′-hydroxyl loop (residues 241−246) moves away from the active site. In the TB-PNP·ImmH·PO_4 complex, His243 directs the 5′-hydroxyl to a syn conformation. The lone pair from O5′ is proposed to play a role in ribooxocarbenium ion formation to form the transition state (*16*). However, the mutation His243Ala decreased k_{cat} by a factor of 4 and k_{cat}/K_m only by a factor of 20 in human PNP (*29*). In the absence of a 5′-hydroxyl group, the side chain of His243 moves

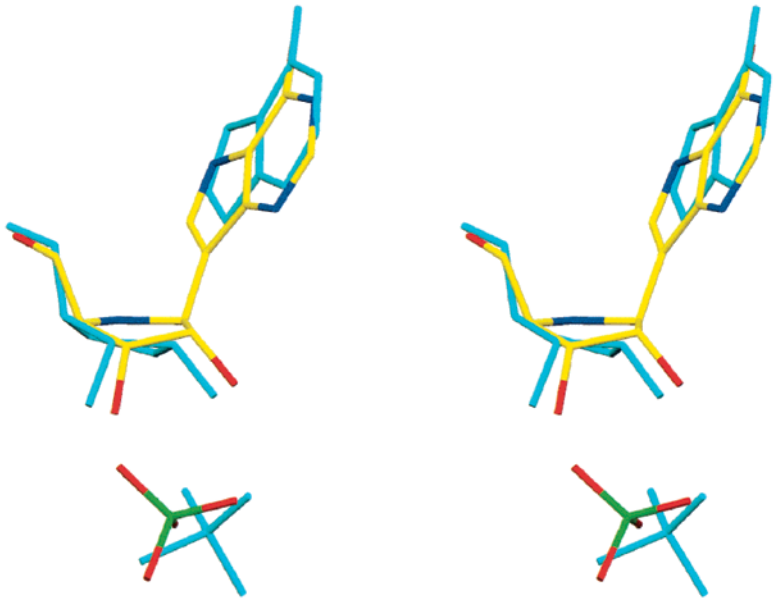

FIGURE 7: Positional comparison of ImmH and PO_4 from the complex of TB-PNP·ImmH·PO_4 with the 9dHX, IR, and PO_4 from the complex of TB-PNP·9dHX·IR·PO_4. Regions of the peptide backbone (amino acids 36, 88−92, 188, 189, 231, 243) that are in the same positions in both complexes described here were used for spatial alignment of the catalytic site components. Removing the C1′−C9 bond of ImmH in the TB-PNP complex causes both phosphate and the purine base to move away from the ribosyl analogue.

approximately 4 Å away from the catalytic site. In the closed transition-state complex of TB-PNP, loop 151−155 from the neighboring subunit closes over the active site and is proposed to remain there during formation of the transition state (the red loop in Figure 6c). The side chain of the intersubunit Phe153 is in van der Waals contact with the O5′−C5′−C4′−C3′−O3′ region of the inhibitor and stacks between Tyr92 and His243 in the TB-PNP·ImmH·PO_4 complex. This residue seals the site of ribooxocarbenium ion formation from solvent access. In subunits with only 9dHX bound, this side chain rotates 90° but maintains a stacking interaction with His243. However, both residues are shifted from this position when ImmH and PO_4 are bound. The binding site for phosphate also shows a major structural change in the absence of bound phosphate. The side chain of Ser36 rotates approximately 180° away from the empty phosphate site (Figure 6a). With phosphate bound, the Ser hydroxyl provides a bridging atom between the nucleophilic phosphate oxygen (O4) and the imino nitrogen in the TB-PNP·9dHX·IR·PO_4 complex. This Ser is also conserved in the mammalian PNP structures (e.g., Figure 4).

The IR and PO_4 Binding Sites in TB-PNP·9dHX·IR·PO_4. Filling the TB-PNP active site with the pieces of the transition-state inhibitor complex resulted in a catalytic site with all components bound in orientations and in hydrogen bond networks related to the complex of TB-PNP·ImmH·PO_4. The distance between C9 of 9dHX and C1 of IR is 3.1 Å, consistent with a van der Waals contact (Figure 4c). Thus, loss of the covalent bond results in this distance increasing by 1.7 Å (from 1.4 to 3.1 Å). The 5-hydroxyl group of IR is in hydrogen bond distance with the side chains of Tyr188 and His243, similar to that observed in the complex of TB-PNP·ImmH·PO_4 (2.6 and 2.8 Å, respectively). The side chain of Tyr92 forms a 2.7 Å hydrogen bond with the 3-hydroxyl group. Phe153 from the neighboring subunit is in van der Waals contact with the O5−C5−C4−C3−O3 atoms of IR. However, the N4−C1−C2−O2 atoms of IR have few interactions with the protein. A consequence of the weak interactions to this region of IR is a loss of structural order compared to the 9dHX (compare Figure 3a,b). Phosphate is also less ordered in the $F_o - F_c$ map (Figure 3b). The *B*-factors for the C, N, and O atoms of 9dHX in the complex range from 8.0 to 13.9 Å^2, while those for IR vary from 30.2 to 38.4 Å^2 and those for phosphate atoms range from 39.2 to 44.4 Å^2.

The imino group N4′ of ImmH confers electrostatic similarity to the oxocarbenium transition state catalyzed by PNP (*15*). In the structures of both *M. tuberculosis* and bovine PNP in complexes with ImmH and PO_4, N4′ is sandwiched between the 5′-hydroxyl oxygen and the negatively charged phosphate (O4) oxygen. These neighboring oxygen groups assist in ribooxocarbenium ion formation since no protein atoms are close enough to N4′ to participate in transition stabilization (Figure 4). But in the TB-PNP·9dHX·IR·PO_4 complex, there are no significant phosphate interactions below the N4 imino group, even though the O5−N4 interaction is maintained. Instead, the side chain of Ser36 orients toward N4 and forms a 2.7 Å H-bond. This interaction could play a role in the reverse reaction of PNP (ribose 1-PO_4 + hypoxanthine → inosine + PO_4) where stabilization of the ribooxocarbenium ion transition state is required and the bridging phosphate oxygen is not available to form the three-oxygen electrostatic sandwich (*9*).

The phosphate ion present in the TB-PNP·9dHX·IR·PO_4 complex showed high *B*-factors and weak electron density in the $F_o - F_c$ maps relative to 9dHX in the same complex (see above). Electron densities for the four oxygen atoms are not well resolved, implying that the phosphate ion is not held rigidly in the active site. The van der Waals contact distance (3.1 Å) between N9 and C1 of IR causes the N4−C1−C2−O2 portion of IR to be shifted lower in the binding pocket, consequently causing the bound phosphate to be positioned lower in the binding pocket. The only phosphate oxygen atom to maintain the hydrogen bond network of the TB-PNP·ImmH·PO_4 complex is O2. This oxygen atom interacts with O2 from IR (2.6 Å), the side chain of Ser208

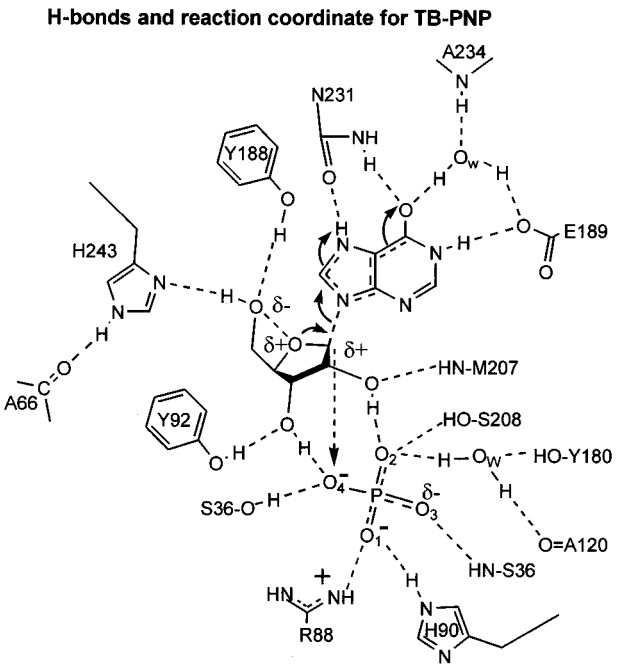

FIGURE 8: Assignments of H-bond acceptor and donor interactions that lead to the transition state for phosphorolysis of inosine by TB-PNP. The arrows indicate electron flow for formation of the transition state. The dashed arrow from C1′ to O4 emphasizes the reaction coordinate motion established previously from studies on the bovine PNP. The purine base and phosphate are held rigidly in the catalytic sites, and the ribosyl oxocarbenium ion migrates between the two groups to achieve forward and reverse catalysis (*9*).

(2.6 Å), and provides a water-mediated hydrogen bond with Tyr180 and Ala120. Although the same amino acid side chains interact with phosphate in both complexes with the bound anion, the participating groups are shifted to different locations. Oxygen O2 thus serves as a pivot point for the movement of phosphate in the catalytic site (Figure 7). A similar motion of phosphate was seen in the complexes of bovine PNP with analogues of substrate, the transition state, and products (*9*). These similar motions of phosphate support a reaction coordinate hinge motion to bring the nucleophilic O4 in position to attack the developing oxocarbenium ion (Figure 8).

Summary and Conclusions. The structure of *M. tuberculosis* PNP in complex with the transition-state analogue inhibitor ImmH and phosphate provides a detailed view of the catalytic conformation of this enzyme near its transition state. The chemical and structural determinants that destabilize bound substrate and stabilize the oxocarbenium ion structure of the transition state are identified, as are the differences that distinguish this enzyme from its bacterial and mammalian counterparts. Significant discoveries include the following: (1) *M. tuberculosis* PNP is structurally more similar to mammalian PNPs than to *E. coli* or *Cellulomonas* PNPs; (2) there is a substrate-assisted catalysis mechanism with the neighboring group hydroxyl and phosphate as major stabilizing factors to the oxocarbenium transition state; (3) there are catalytic loop segments close to the active site in the complex with the bound transition-state analogue, accompanied by the formation of numerous favorable hydrogen bonds; (4) a significant difference in the hydrogen bond pattern to ImmH between mammalian and *M. tuberculosis* PNPs suggests that isozyme-specific inhibitor design may be possible.

A complex of *M. tuberculosis* PNP with the pieces of the transition state reveals interactions that are both dependent and independent on the intact transition-state analogue. Contacts to the isolated purine leaving group and to the hydroxymethyl group of iminoribitol are similar for the intact transition-state analogue inhibitor or its pieces. However, the ribosyl analogue and the phosphate groups show loose environments and weakened H-bonding patterns. The results confirm the proposal that the reaction coordinate motion involves migration of the C1 portion of a ribosyl oxocarbenium ion but emphasizes that immobilization and activation of the phosphate are dependent on the ribosyl link to the purine. Loss of this connection permits the enzyme to relax in the direction of the reaction coordinate motion, and the apposition of the catalytic groups does not occur as it would in the transition state.

REFERENCES

1. Raviglione, M. C., Snider, D. E., Jr., and Kochi, A. (1995) *J. Am. Med. Assoc. 273*, 220−226.
2. Cole, S. T., Brosch, R., Parkhill, J., Garnier, T., Churcher, C., Harris, D., et al. (1998) *Nature 393*, 537−544.
3. Valway, S. E., Sanchez, M. P., Shinnick, T. F., Orme, I., Agerton, T., Hoy, D., Jones, J. S., Westmoreland, H., and Onorato, I. M. (1998) *N. Engl. J. Med. 338*, 633−639.
4. Giblett, E. R., Ammann, A. J., Wara, D. W., Sandman, R., and Diamond, L. K. (1975) *Lancet 1*, 1010−1013.
5. Stoeckler, J. D. (1984) in *Developments in Cancer Chemotherapy* (Glazer, R. J., Ed.) pp 35−60, CRC Press Inc., Boca Raton, FL.
6. Montgomery, J. A., Niwas, S., Rose, J. D., Secrist, J. A., III, Babu, Y. S., Bugg, C. E., Erion, M. D., Guida, W. C., and Ealick, S. E. (1993) *J. Med. Chem. 36*, 55−69.
7. Ealick, S. E., Rule, S. A., Carter, D. C., Greenhough, T. J., Babu, Y. S., Cook, W. J., Habash, J., Helliwell, J. R., Stoeckler, J. D., Parks, R. E., Jr., Chen, S. F., and Bugg, C. E. (1990) *J. Biol. Chem. 265*, 1812−1820.
8. Mao, C., Cook, W. J., Zhou, M., Federov, A. A., Almo, S. C., and Ealick, S. E. (1998) *Biochemistry 37*, 7135−7146.
9. Fedorov, A., Shi, W., Kicska, G., Fedorov, E., Tyler, P. C., Furneaux, R. H., Hanson, J. C., Gainsford, G. J., Larese, J. Z., Schramm, V. L., and Almo, S. C. (2001) *Biochemistry 40*, 853−860.
10. Tebbe, J., Arnieszka, B., Wielgus-Kutrowska, B., Schroder, W., Kazimierczuk, Z., Shugar, D., Saenger, W., and Koellner, G. (1999) *J. Mol. Biol. 294*, 1239−1255.
11. Mao, C., Cook, W. J., Zhou, M., Koszaka, C. W., Krenitsky, T. A., and Ealick S. E. (1997) *Structure 5*, 1373−1383.
12. Koeller, G., Luic, M., Shugar, D., Saenger, W., and Bzowska, A. (1998) *J. Mol. Biol. 280*, 153−166.
13. Kline, P. C., and Schramm, V. L. (1993) *Biochemistry 32*, 13212−13219.
14. Kline P. C., and Schramm V. L. (1995) *Biochemistry 34*, 1153−1162.
15. Miles, R. W., Tyler, P. C., Furneaux, R. H., Bagdassarian, C. K., and Schramm, V. L. (1998) *Biochemistry 37*, 8615−8621.
16. Basso, L. A., Santos, D. S., Shi, W., Furneaux, R. H., Tyler, P. C., Schramm, V. L., and Blanchard, J. S. (2001) *Biochemistry 40*, 8196−8203.
17. Otwinowski, Z., and Minor, W. (1997) *Methods Enzymol. 276*, 307−326.
18. Navaza, J. (1994) *Acta Crystallogr. A50*, 157−163.
19. Brunger, A. T. (1992) *X-PLOR Version 3.1*, Yale University Press, New Haven, CT.
20. Jones T. A. (1985) *Methods Enzymol. B115*, 157−171.

21. Laskowski, R. A., MacArthur, M. W., and Thornton, J. M. (1993) *J. Appl. Crystallogr. 26*, 283−291.
22. Sheriff, S., Hendrickson, W. A., and Smith, J. L. (1987) *J. Mol. Biol. 197*, 273−296.
23. Horenstein, B. A., and Schramm, V. L. (1993) *Biochemistry 32*, 9917−9925.
24. Degano, M., Almo, S. C., Sacchettini, J. C., and Schramm, V. L. (1998) *Biochemistry 37*, 6277−6285.
25. Berti, P. J., and Schramm, V. L. (1997) *J. Am. Chem. Soc. 119*, 12069−12078.
26. Shi, W., Li, C. M., Tyler, P. C., Furneaux, R. H., Grubmeyer, C., Schramm, V. L., and Almo, S. C. (1999) *Nat. Struct. Biol. 6*, 588−593.
27. Shi, W., Li, C. M., Tyler, P. C., Furneaux, R. H., Cahill, S. M., Girvin, M. E., Grubmeyer, C., Schramm, V. L., and Almo, S. C. (1999) *Biochemistry 38*, 9872−9880.
28. Wang, F., Miles, R. W., Kicska, G., Nieves, E., Schramm, V. L., and Angeletti, R. H. (2000) *Protein Sci. 9*, 1660−1668.
29. Erion, M. D., Takabayashi, K., Smith, H. B., Kessi, J., Wagner, S., Honger, S., Shames, S. L., and Ealick, S. E. (1997) *Biochemistry 36*, 11725−11734.
30. Fleet, G. W. J., and Son, J. C. (1988) *Tetrahedron 44*, 2637−2647.
31. Evan, S. V. (1993) *J. Mol. Graphics 11*, 134−138.

BI010585P